Nanowire Solar Cells: A New Radiation Hard PV Technology for Space Applications

Pilar Espinet-Gonzalez, Enrique Barrigón, Yang Chen, Gaute Otnes, Giuliano Vescovi, Colin Mann, John V. Lloyd, Don Walker, Michael D. Kelzenberg, Ingvar Åberg, Magnus Borgström, Lars Samuelson, and Harry A. Atwater

***Abstract*—Radiation hard thin-film solar cell technologies are necessary in order to achieve a step forward in the specific power of solar arrays for space applications. In this article, we analyze the degradation of nanowire (NW) solar cells under high energy particles. GaAs NW solar cells have been irradiated with protons of 100 and 350 keV at different fluences. The radiation hardness of the NW solar cells in all the cases is remarkable in comparison with GaAs planar solar cells and prior literature. Design guidelines to optimize the specific power of NW solar cells for space applications by jointly increasing their efficiency and radiation hardness are presented.**

***Index Terms*—Binary collision approximation, Monte Carlo simulations, nanostructured materials, nanowire solar cells, radiation hard, space environment, space solar cells.**

I. Introduction

III-V multijunction solar cells are the dominant solar cell technology for space applications. The high efficiency achieved ($\sim$32% [1], [2]) and their proven reliability in the space environment have made them the leader in the space market. Furthermore, in the last decade a significant effort has been put into increasing the power-to-weight ratio (W/g); the so-called *specific power* of the solar arrays, by thinning/eliminating [3], [4] the nonactive substrate of the multijunction solar cells and packaging them into light-weight flexible polyimide substrates. However, the specific power that multijunction solar cells can achieve is ultimately limited by the shielding required to protect them against high energy particles [5]. Typical arrays utilize $>$75 μm of ceria-doped cover glass in front of the cells, and a similar mass backing the cells, to reduce radiation damage. Therefore, in order to dramatically increase the specific power of space solar arrays, particularly in proton-dominated orbits, a radiation-tolerant thin-film solar cell technology is desired. Studies have reported promising radiation hardness in thin-film solar cell technologies such as CIGS [6], CdTe [7], and perovskite [8] solar cells. Also, work toward device engineering on the well-known III-V materials has been carried out. In particular, light trapping strategies combined with a drastic reduction of thickness in the GaAs absorber (thickness $\sim$100 nm) have been studied as a way of increasing the radiation resistance of III-V solar cells [9]. Furthermore, quantum dots and quantum well subcells have been included in III-V multijunction architectures in order to improve end-of-life current matching.

In this line of enhancing the radiation resistance of the otherwise highly reliable and efficient III-V materials, we have studied the performance of III-V nanowire (NW) solar cells under the radiation of high energy particles. The efficiency of bottom-up NW solar cells has been increasing over the last decade with values as high as 15.3% for GaAs [11] and 15.0% for InP [12] and up to 17.8% for etched down InP NW solar cells [13] for AM1.5G [14].

In this article, the radiation hardness of GaAs NW solar cells has been evaluated by irradiating them with protons (100 and 350 keV) at three different fluences, and their behavior has been compared with planar devices. Design considerations for high efficiency, radiation tolerant NW space solar cells are presented.

II. Solar Cells

Two different solar cell technologies have been manufactured and included in the irradiation tests: GaAs NW solar cells and epitaxial lift-off (ELO) planar GaAs solar cells. The GaAs NW solar cells consist of a parallel connection of millions of single, vertical, high-aspect-ratio semiconductor structures (NWs) with a low surface coverage ($\sim$8%). The NWs have an $\sim$80 nm radius, a 500 nm square pitch (distance between the midpoints of two adjacent wires), and $\sim$3–3.2 μm length. They are surrounded by an $Al_{0.9}Ga_{0.1}As$ shell to minimize the high surface recombination in the GaAs surface. Once grown, a conformal insulating SiO_x

Manuscript received June 20, 2019; revised December 16, 2019; accepted January 7, 2020. Date of publication January 31, 2020; date of current version February 19, 2020. This work was supported in part by Northrop Grumman, in part by the Space Solar Power Project, in part by Knut and Alice Wallenberg Foundation, and in part by the European Union's Horizon 2020 research and innovation programme under Grant 641023 (Nano-Tandem) and under the Marie Sklodowska-Curie Grant 656208. *(Corresponding author: Harry A. Atwater.)*

P. Espinet-Gonzalez, J. V. Lloyd, M. D. Kelzenberg, and H. A. Atwater are with the California Institute of Technology, Pasadena, CA 91101 USA (e-mail: pespinet@caltech.edu; john.v.lloyd@gmail.com; mdk@caltech.edu; haa@caltech.edu).

E. Barrigón, Y. Chen, G. Otnes, and M. Borgström are with the Division of Solid State Physics and NanoLund, Lund University, SE-221 00 Lund, Sweden (e-mail: enrique.barrigon@ftf.lth.se; yang.chen@ftf.lth.se; gaute.otnes@ife.no; magnus.borgstrom@ftf.lth.se).

G. Vescovi and I. Åberg are with the Sol Voltaics AB, 223 63 Lund, Sweden (e-mail: gpvescovi@gmail.com; iaberg@alum.mit.edu).

C. Mann and D. Walker are with the The Aerospace Corporation, El Segundo, CA 90245 USA (e-mail: colin.j.mann@aero.org; don.walker@aero.org).

L. Samuelson is with the Division of Solid State Physics and NanoLund, Lund University, SE-221 00 Lund, Sweden, and also with Sol Voltaics AB, 223 63 Lund, Sweden (e-mail: lars.samuelson@ftf.lth.se).

Color versions of one or more of the figures in this article are available online at https://ieeexplore.ieee.org.

Digital Object Identifier 10.1109/JPHOTOV.2020.2966979

TABLE I
DEGRADATION RATIO SUMMARY OF THE DIFFERENT SOLAR CELL TECHNOLOGIES IN EACH EXPERIMENT

		NW		planar
p^+/cm^2	Parameter	100 keV	350 keV	350 keV
10^{10}	J_{sc}/J_{sc0}	-	1.07±0.05	0.98±0.02
	V_{oc}/V_{oc0}	-	1.00±0.01	0.91±0.04
10^{11}	J_{sc}/J_{sc0}	0.95±0.02	0.99±0.02	0.83±0.02
	V_{oc}/V_{oc0}	0.90±0.01	0.97±0.01	0.68±0.02
$5{\cdot}10^{11}$	J_{sc}/J_{sc0}	0.88±0.03	-	-
	V_{oc}/V_{oc0}	0.81±0.01	-	-
10^{12}	J_{sc}/J_{sc0}	0.72±0.03	0.94±0.02	0.11±0.02
	V_{oc}/V_{oc0}	0.80±0.01	0.83±0.01	0.45±0.01

layer is deposited around the core-shell NWs. Subsequently, the array is filled-in with Cyclotene resin, the Au catalyst particle used to grow the wires is etched down and indium tin oxide (ITO) is deposited to connect the n-type top side of the NWs in parallel. After that, standard photolithography techniques are used to process the NWs array into solar cells of 1.049 mm^2 area and to define a Ti/Au busbar as described in detail in [11]. The efficiency of the fabricated GaAs NW solar cells included in the irradiation tests is ∼11.6% ± 0.9% at terrestrial spectrum AM1.5G. Planar GaAs solar cells have been included as controls for the 350 keV proton testing. The total epitaxial thickness is ∼4.4 μm and they have been lifted off from their GaAs growth substrates as described in [15] and processed into 8.4 mm^2 solar cells without an antireflecting coating. The efficiency of the ELO GaAs solar cells before the irradiation tests is ∼15.7% ± 1.0% at terrestrial spectrum AM1.5G.

III. IRRADIATION TEST

The solar cells were irradiated with protons at The Aerospace Corporation with energies of 100 keV ($1{\cdot}10^{11}$ p^+/cm^2, $5{\cdot}10^{11}$ p^+/cm^2, and $1{\cdot}10^{12}$ p^+/cm^2) and 350 keV ($1{\cdot}10^{10}$ p^+/cm^2, $1{\cdot}10^{11}$ p^+/cm^2, and $1{\cdot}10^{12}$ p^+/cm^2). The irradiation tests were carried out in vacuum (10^{-6} Torr) at room temperature with a normal incidence proton flux of $6{\cdot}10^7$ $p^+/cm^2{\cdot}s$. Stopping and range of ions in matter (SRIM) simulations (not shown here) estimate that the penetration depths for 100 and 350 keV protons in GaAs are ∼750 nm and ∼2.7–2.9 μm, respectively. Therefore, in both cases the protons are expected to stop within the devices causing severe damage.

At each fluence and energy tested a different sample containing several (3–5) similar performing solar cells from the same growth and processing batch were included. Therefore, a different set of solar cells were included in each of the fluences tested. The light J–V curves and dark I–V curves of each cell were measured before and after the irradiation tests at room temperature. The solar simulator set up was calibrated to AM1.5G using a reference Si solar cell. In order to have a higher control on the spectrum Spectrolab XTJ top cell (GaInP) and middle cell (GaInAs) isotypes were used, which measured 0.5 suns (AM0) and 0.9 suns (AM0), respectively. Table I summarizes the degradation ratio of the short-circuit current (J_{sc}/J_{sc0}) and

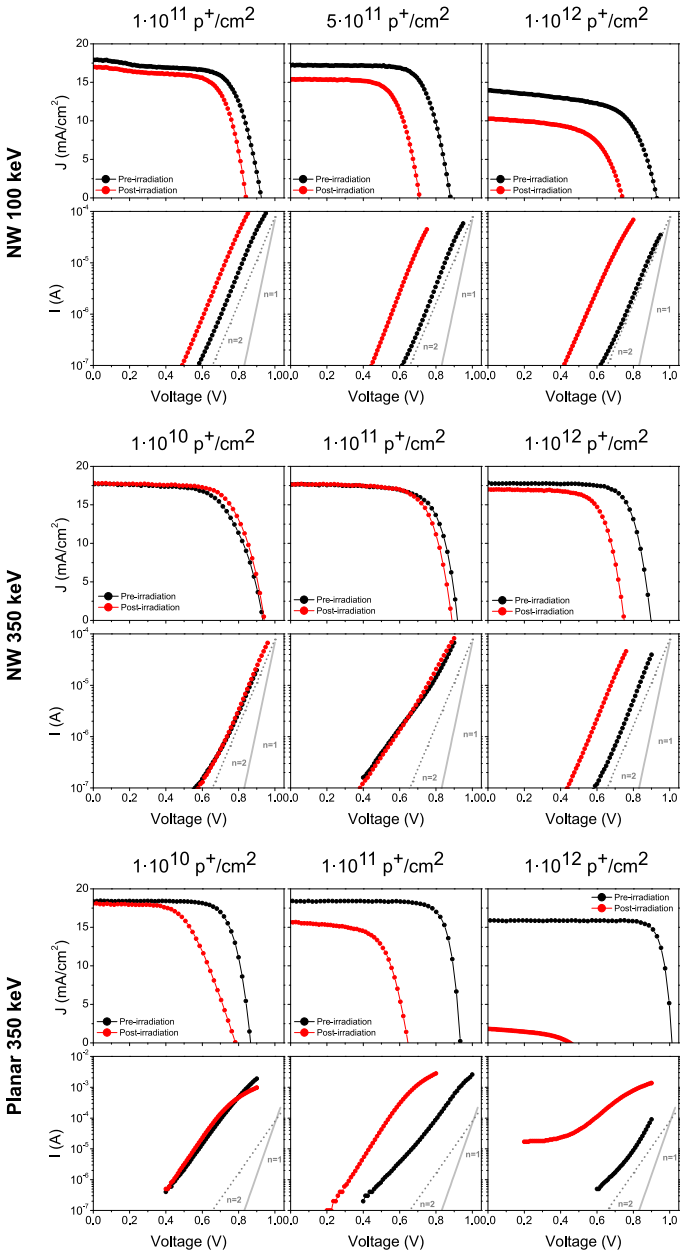

Fig. 1. Light J–V and dark I–V curves of representative solar cells before and after the irradiation test.

open-circuit voltage (V_{oc}/V_{oc0}) after the different irradiation experiments and Fig. 1 shows the evolution of the I–V curves before and after the irradiation of representative devices.

A commensurate degradation rate of the short-circuit current density (J_{sc}) and open-circuit voltage (V_{oc}) have been reported in space planar GaAs solar cells by Anspaugh [16] but at a fluence ∼10 times lower than for GaAs NW solar cells manifesting the radiation robustness of the NW array architecture. For instance, the V_{oc} and J_{sc} remaining factors after a fluence of 10^{10} p^+/cm^2 is ∼ 0.9 and ∼0.95, respectively, in the planar space solar cells [16] irradiated with 100 keV, meanwhile this decay is observed in the GaAs NWs at a fluence of 10^{11} p^+/cm^2. The irradiation with 100 keV causes a left shift of the dark I–V curves. The

postirradiation dark I–V curves of the NW solar cells present an ideality factor n∼2, which is symptomatic of solar cells dominated by Shockley-Read-Hall recombination localized in either the depletion region or at the surface [17].

At 350 keV, the GaAs NW solar cells show a degradation threshold ∼40 times higher than the planar ELO GaAs solar cells included in the same test. Thus, demonstrating again the superior radiation hardness of the NW architecture. For the ELO cells, Fig. 1 shows that 350 keV protons at a fluence of just 10^{10} p^+/cm^2 causes a ∼10% drop in V_{oc} and a significant increase in the series resistance in both the light and the dark I–V curves. As the proton fluence increases to 10^{11} p^+/cm^2, the voltage drop increases (>30%) and the degradation in short-circuit current is also significant (>15%) meanwhile only a slight decrease in V_{oc} (∼3%) is observed in the NW solar cells. At the highest fluence tested, 10^{12} p^+/cm^2, the J_{sc} and V_{oc} of the ELO solar cells have dropped dramatically. The corresponding dark I–V curve reveals a low shunt resistance, a high series resistance, and a high saturation current density with an ideality factor >2. On the contrary, the degradation of the NW solar cells at 10^{12} p^+/cm^2 is still moderate with a small loss in J_{sc} (∼6%) and a drop <20% in V_{oc}. The same evolution of the dark I–V curves as in the irradiation with 100 keV protons is observed. There is no apparent increase in series resistance affecting the fill factor or dark I–V curves, and while the saturation current density increases as the fluence is higher the ideality factor remains ∼2.

In conclusion, NW solar cells have shown superior radiation resistance to both 100 and 350 keV proton energies. Shielding is used in standard space solar cells to reduce the fluence of highly damaging energies, which stop within the semiconductor device such as the energies tested. The superior radiation hardness demonstrated by the NW solar cells implies that the amount of shielding that they would require to operate in space might be reduced, or alternately, the duration of the missions could be extended.

IV. Specific Power Optimization

NWs can achieve high light absorption because of resonant light trapping if the geometry of the array is properly designed [18]. In order to maximize the specific power of NW solar cells, the array geometry needs to be designed taking into account both the light absorption to maximize the sunlight power conversion efficiency and the radiation hardness. In this manner, we have explored the impact that different NW array designs have on efficiency and radiation hardness.

The J_{sc} under the extraterrestrial solar spectrum (AM0) for different square NW array geometries has been calculated using the scattering matrix method [18] and assuming perfect carrier collection. In all the cases, the GaAs NWs simulated are 3 μm long and they are surrounded by a 20 nm thick AlAs shell for passivating the surface of the NWs and a 20 nm thick insulating layer of SiO_2 covering the core-shell NWs radially as shown in Fig. 2. The array is planarized by infilling the NWs with benzocyclobutene (BCB) to resemble the structural configuration of the final device. In the optical simulations, the front medium considered is air (n = 1) and the back medium is GaAs (n = 3.5).

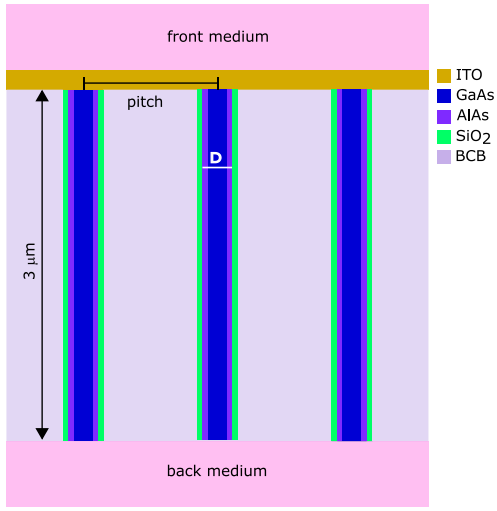

Fig. 2. Sketch of the NW arrays simulated with variable pitch (p) and diameter (D, D = GaAs core + 2·20 nm AlAs).

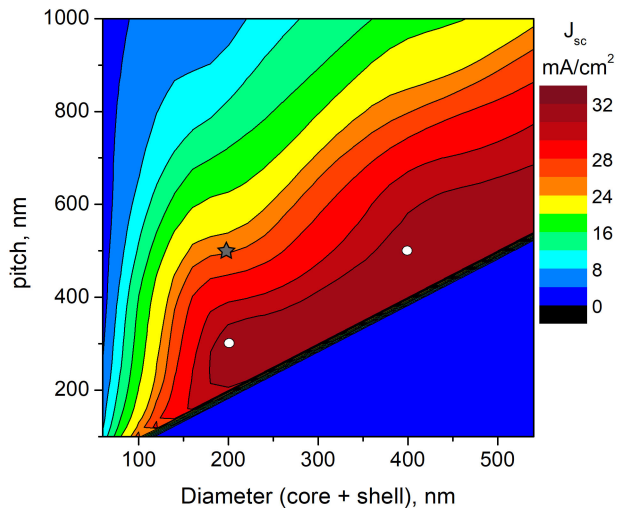

Fig. 3. J_{sc} of GaAs NW solar cells as a function of the wire pitch and NW diameter (GaAs + AlAs). The white circles mark two different NW geometries with the same high optical absorption and the gray star denotes the NW geometry of the solar cells fabricated and tested.

Fig. 3 represents the short-circuit current generated as a function of the NWs diameter (variable GaAs diameter + 2·20 nm AlAs shell) and pitch. Fig. 3 shows that similar J_{sc} values can be obtained with significantly different geometries such as the two points highlighted with a white circle. Also, the NW array resembling the solar cells irradiated has been marked in Fig. 3 with a gray star to include in the analysis.

As shown in the irradiation tests, the NW geometry also has a profound effect on the radiation damage experienced by the semiconductor material. There are primarily three possible mechanisms by which the NW geometry improves radiation tolerance. First, because the wire arrays are sparse and infilled with a different density inactive material, the high energy protons or secondary recoils might tend to scatter out of the NWs into the infill material or vice versa, effectively changing the protons

cross section for defect production versus planar materials and the irradiation induced damage profile as explained in [19]. Second, as reported in the literature [20], the dynamics of the collision cascades ("heat spiking") can give rise to enhanced dynamic annealing of defects in nanoscale systems and it has been shown experimentally in Ge [21] and GaN NWs [22]. Third, the surfaces and interfaces can influence the dynamics of the irradiation-induced point defects favoring their annihilation [23], [24]. Here, we evaluate the effects of the former, the array geometry implications on the damage distribution. In planar 2-D systems, the damage induced by high energy protons is typically analyzed with Monte Carlo programs such as TRIM/SRIM [26]. The Monte Carlo simulation codes using the binary collision approximation assume that ions travel in a straight line between collisions experiencing stopping power. In a collision, the classical scattering integral is solved and the secondary recoils are followed, thus obtaining the distributions of the ions in the target and the displacements (vacancies and interstitials) induced. To simulate these effects for the 3-D NW geometry under proton irradiation, we have used iradina [27]. The distribution of Arsenic atoms displaced from its site within the crystal lattice, which has been reported to be the primary irradiation-induced defect in GaAs solar cells [28], have been calculated.

Four different solar cell architectures, all of them 3 μm thick, have been compared: first, a planar GaAs slab, second, a NW array with a NW diameter (GaAs core + AlAs shell) = 200 nm and pitch = 300 nm (packing fraction = 35%), third, a NW array with core diameter = 400 nm and pitch = 500 nm (packing fraction = 50%), and last, a NW array with core diameter = 200 nm and pitch = 500 nm (packing fraction = 13%). Thus, the planar architecture is contrasted with the two optimum arrays marked with a white circle in Fig. 3 and with one suboptimal geometry in terms of light absorption (gray star in Fig. 3) but with a considerably lower surface coverage resembling the devices tested experimentally. The NW arrays simulated with Monte Carlo have the geometry depicted in Fig. 2 with vacuum for the front and back medium. In order to enable a direct comparison between the radiation performance of the planar and the NW architectures, both of them contain a 100 nm thick ITO film on top. Periodic boundary conditions are assumed laterally in the Monte Carlo simulations to emulate an infinite solar array. The displacement energy assumed for Ga, As, and Al in the simulations is 10 eV in all the cases. Finally, the NWs collect light from the entire NW array area, and not only from their physical cross section. Therefore, in order to avoid underestimating the degradation in NW solar cells, the Arsenic displacements originated in the NW array have been integrated (see Fig. 4) or averaged (see Fig. 5) exclusively over the area covered by GaAs.

The induced damage (#As displacements/Å·ion) in the different architectures as a function of proton energy is represented in Fig. 4(a). In the planar case, the As displacements increase with proton energy up to ~360 keV. At energies above this, the protons can fully penetrate the GaAs slab without imparting the entirety of their energy, thus, reducing abruptly the damage originated in the device. Fig. 4(a) shows that the scattering events in the NW array favor the protons to stop in the infilling material

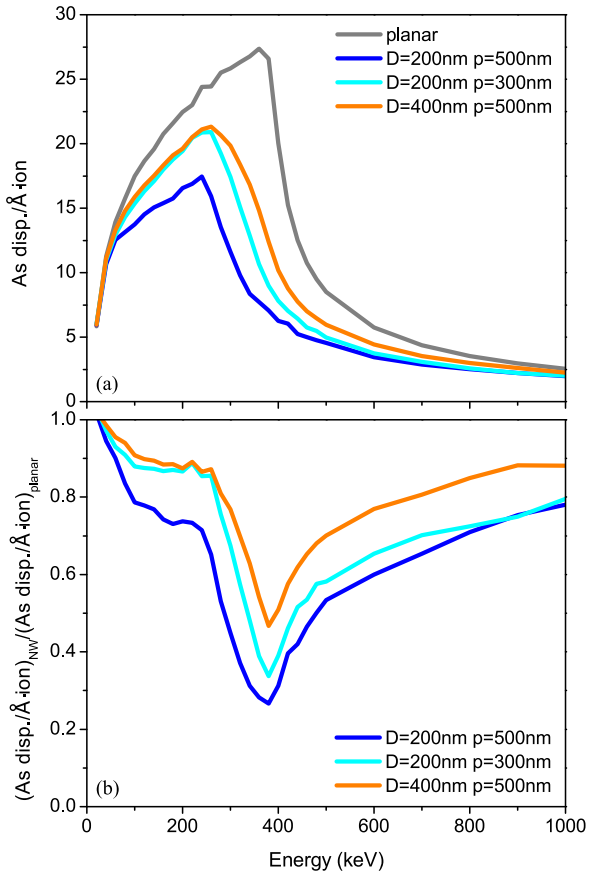

Fig. 4. (a) Damage in the GaAs (As disp./Å·ion) originated in different solar cell geometries under different protons energies. (b) Induced-damage ratio of planar to NW ratio.

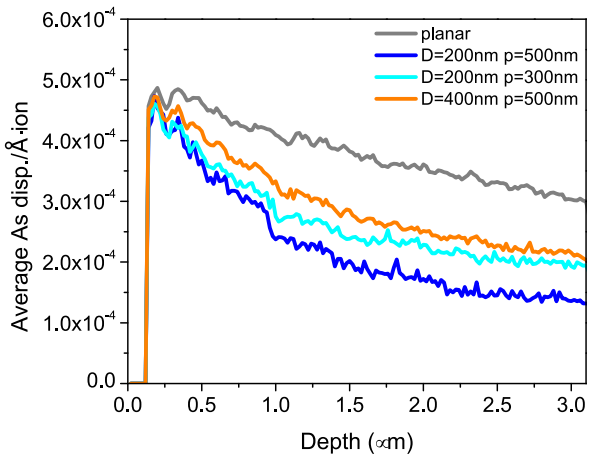

Fig. 5. Average induced-damage distribution within the planar slab and the NWs when irradiating the structures with normal incidence protons of energies ranging from 20 keV to 1 MeV.

(BCB) or to leave the array without depositing their energy on the NWs as explained in detail in [19]. The Arsenic displacements in the different NW arrays normalized to the Arsenic displacements in the planar case as a function of different proton energies are represented in Fig. 4(b). The NW geometry reduces the damage produced by protons ($\text{damage}_{\text{NW}}/\ \text{damage}_{\text{planar}} < 1$) for all

the NW array geometries and proton energies simulated, particularly at the most harmful energies [280–500 keV Fig. 4(a)]. Therefore, the Monte Carlo simulations evidence a benefit of the NW solar cell tested (diameter = 200 nm and pitch = 500 nm) with a ∼20% and ∼70% lower damage at 100 and 350 keV, respectively, than in the planar architecture. However, the radiation resistance observed in the NW solar cells in the irradiation tests by far surpasses the Monte Carlo estimations with a damage ∼10-fold and 40-fold lower than the ELO planar GaAs solar cells [19]. Therefore, other factors such as dynamic thermal annealing and annihilation of the defects at the interfaces might be playing a significant role.

In the design of radiation hard NW arrays, Fig. 4(b) suggests that the thinner and the sparser the wires the better. The array made of NWs with a dimeter of 200 nm and a pitch of 500 nm is the most radiation hard design at the expense of a significant penalty on the J_{sc}. On the other hand, the impact of the diameter on the V_{oc} can be assumed negligible in NWs with a low surface recombination velocity. However, thin wires might suffer from a lower V_{oc} when the surface recombination velocity is high [17]. Therefore, when designing NW arrays for high specific power (W/g) solar cells, the mass for shielding and the cell performance need to be carefully estimated.

Fig. 5 shows the in-depth average damage induced predicted by Monte Carlo simulations when the devices are irradiated with normal incidence protons with a spectrum of energies ranging from 20 keV to 1 MeV. For simplicity, all the energies have equal weight. The simulations predict that in order to produce the same damage in the NWs arrays as in the planar slab the fluence on the NW arrays should be 1.68 x $\text{fluence}_{\text{planar}}$ for the case D = 200 nm, p = 500 nm, 1.42 x $\text{fluence}_{\text{planar}}$ in the case of D = 200 nm, p = 300 nm and 1.29 x $\text{fluence}_{\text{planar}}$ for D = 400 nm, p = 500 nm. As pointed out previously, it has been proven experimentally that the radiation hardness of the NW arrays, at least at proton energies with a penetration depth in GaAs shorter than the length of the NWs, is considerably higher than the values obtained by Monte Carlo simulations. Therefore, the radiation hardness advantage obtained from Fig. 5 should be considered a lower limit to the radiation resistance potential of NW arrays.

V. Summary and Conclusion

We have found that III-V NW solar cells have exceptionally promising radiation tolerance with respect to high energy particle radiation in the space environment. GaAs NW solar cells have been irradiated with 100 and 350 keV protons, and in all the cases, the NW solar cells outperformed the radiation resistance of planar cells published in the literature or included in the same radiation tests. The radiation hardness exhibited by the NW solar cells make them an attractive solar cell technology able to achieve a high specific power and long life in space applications. Simulations of optical absorption and proton irradiation damage in GaAs NW arrays suggest that the specific power of NW solar cells can be enhanced by the optimization of the array geometry by favoring high efficiency designs with thin and separated wires. Further experimental tests to evaluate the impact of omnidirectional radiation in the NW array geometry as well as the effects of higher energy protons end electrons that cross the entire device are required in order to quantify the benefit of NW architectures for different space environments.

Acknowledgment

The work performed within NanoLund was supported by the Swedish Research Council (Vetenskapsrådet), Swedish Foundation for Strategic Research (SSF), and Swedish Energy Agency. This article reflects only the authors' views and the funding agency is not responsible for any use that may be made of the information it contains. The authors acknowledge the helpful contributions of J. V. Lloyd with the solar cell processing of the ELO GaAs solar cells at Caltech. They also acknowledge The Aerospace Corporation for the irradiation test with protons.

References

[1] 2019. [Online]. Available: https://www.spectrolab.com/photovoltaics/XTE_32_Percent.pdf
[2] 2018. [Online]. Available: https://solaerotech.com/wp-content/uploads/2018/04/IMM-alpha-Preliminary-Datasheet-April-2018-v.1.pdf
[3] D. C. Law *et al.*, "Lightweight, flexible, high-efficiency III-V multijunction cells," in *Proc. IEEE 4th World Conf. Photovolt. Energy Conf.*, Waikoloa, HI, USA, 2006, pp. 1879–1882.
[4] B. M. Kayes, L. Zhang, R. Twist, I-K. Ding, and G. S. Higashi, "Flexible thin-film tandem solar cells with >30% efficiency," *IEEE J. Photovolt.*, vol. 4, no. 2, pp. 729–733, Mar. 2014.
[5] P. Espinet-Gonzalez *et al.*, "Inverted metamorphic triple-junction solar cells on polyimide substrate for concentrator photovoltaic systems in space," in *Proc. 45th IEEE Photovoltaic Specialist Conf.*, Waikaloa, HI, USA, 2018.
[6] M. Yamaguchi, "Radiation-resistant solar cells for space use," *Sol. Energy Mater. Sol. Cells*, vol. 68, no. 1, pp. 31–53, 2001.
[7] J. R. Woodyard and G. A. Landis, "Radiation resistance of thin-film solar cells for space photovoltaic power," *Solar Cells*, vol. 31, no. 4, pp. 297–329, 1991.
[8] J. S. Huang *et al.*, "Effects of electron and proton radiation on perovskite solar cells for space solar power application," in *Proc. IEEE 44th Photovolt. Specialist Conf. (PVSC)*, Washington, DC, USA, 2017, pp. 1248–1252.
[9] L. C. Hirst *et al.*, "Intrinsic radiation tolerance of ultra-thin GaAs solar cells," *Appl. Phys. Lett.*, vol. 109, no. 3, 2016, Art. no. 033908.
[10] C. Kerestes *et al.*, "Radiation effects on quantum dot enhanced solar cells," *Proc. of SPIE*, vol. 8256, 2012, Art. no.82561I-1.
[11] I. Åberg *et al.*, "A GaAs nanowire array solar cell with 15.3% efficiency at 1 Sun," *IEEE J. Photovolt.*, vol. 6, no. 1, pp. 185–190, Jan. 2016.
[12] G. Otnes *et al.*, "Understanding InP nanowire array solar cell performance by nanoprobe-enabled single nanowire measurements," *Nano Lett.*, vol. 18, no. 5, pp. 3038–3046, 2018.
[13] D. van Dam *et al.*, "High-efficiency nanowire solar cells with omnidirectionally enhanced absorption due to self-aligned indium–tin–oxide Mie scatterers," *ACS Nano*, vol. 10, no. 12, pp. 11414–11419, 2016.
[14] E. Barrigón, M. Heurlin, Z. Bi, B. Monemar, and L. Samuelson, "Synthesis and applications of III–V nanowires," *Chem. Rev.*, vol. 119, no. 15, pp. 9170–9220, 2019.
[15] C. Youtsey *et al.*, "Epitaxial lift-off of large-area GaAs thin-film multijunction solar cells," in *Proc. CS MANTECH Conf.*, Boston, MA, USA, , 2012, pp. 347–349.
[16] B. E. Anspaugh, "Proton and electron damage coefficients for GaAs/Ge solar cells," in. *Proc. 22nd IEEE Photovoltaic Specialists Conf.*, Las Vegas, NV, USA, 1991, vol. 2, pp. 1593–1598.
[17] Y. Chen, P. Kivisaari, M.-E. Pistol, and N. Anttu, "Optimized efficiency in InP nanowire solar cells with accurate 1D analysis," *Nanotechnology*, vol. 29, , 2018, Art. no. 045401.
[18] N. Anttu and H. Q. Xu, "Efficient light management in vertical nanowire arrays for photovoltaics," *Opt. Express*, vol. 21, no. S3, pp. A558–A575, 2013.
[19] P. Espinet-Gonzalez *et al.*, "Radiation tolerant nanowire array solar cells," *ACS Nano*, vol. 13, no. 11, pp. 12860–12869, 2019.

[20] A. V. Krasheninnikov and K. Nordlund, "Ion and electron irradiation-induced effects in nanostructured materials," *J. Appl. Phys.*, vol. 107, no. 7, 2010, Art. no. 071301.
[21] M. M. Koleśnik-Gray *et al.*, "In operandi observation of dynamic annealing: A case study of boron in germanium nanowire devices," *Appl. Phys. Lett.*, vol. 106, no. 23, 2015, Art. no. 233109.
[22] S. Dhara *et al.*, "Enhanced dynamic annealing in Ga^{+} ion-implanted GaN nanowires," *Appl. Phys. Lett.*, vol. 82, no. 3, pp. 451–453, 2003.
[23] X.-M. Bai, A. F. Voter, R. G. Hoagland, M. Nastasi, and B. P. Uberuaga, "Efficient annealing of radiation damage near grain boundaries via interstitial emission," *Science*, vol. 327, no. 5973, pp. 1631–1634, 2010.
[24] F. Li *et al.*, "Enhancement of radiation tolerance in GaAs/AlGaAs core–shell and InP nanowires," *Nanotechnology*, vol. 29, no. 22, 2018, Art. no. 225703.
[25] F. Li *et al.*, "Radiation effects on GaAs/AlGaAs core/shell ensemble nanowires and nanowire infrared photodetectors," *Nanotechnology*, vol. 28, no. 12, 2017, Art. no. 125702.
[26] J. F. Ziegler, M. D. Ziegler, and J. P. Biersack, "SRIM – The stopping and range of ions in matter (2010)," *Methods Phys. Res. Sect. B: Beam Interact. Mater. Atoms*, vol. 268, no. 11–12, pp. 1818–1823, 2010.
[27] C. Borschel and C. Ronning, "Ion beam irradiation of nanostructures – A 3D Monte Carlo simulation code," *Nucl. Instrum. Methods Phys. Res. Sect. B: Beam Interact. Mater. Atoms*, vol. 269, no. 19, pp. 2133–2138, 2011.
[28] D. Pons and J. C. Bourgoin, "Irradiation-induced defects in GaAs," *J. Phys. C: Solid State Phys.*, vol. 18, no. 20, pp. 3839–3871, 1985.